J. Fluid Mech. (1967), *vol.* 27, *part* 3, *pp.* 561–580
Printed in Great Britain

The interaction of a fibre tangle with an airflow

By PAUL A. TAUB
General Applied Science Laboratories, Westbury, N.Y.

(Received 9 December 1965 and in revised form 21 March 1966)

An analytical model of the interaction of a fibre tangle with an airflow is proposed. This model replaces the discrete fibres by a continuum medium with a non-linear stress–strain law. The governing equations have been examined for one-dimensional unsteady flow configurations and have been found to possess five characteristic directions.

A numerical-solution procedure, based upon the method of characteristics, has been outlined and applied to the flow within a dilation chamber. A fibre sample is located at the centre of the chamber, which is alternately pressurized and depressurized.

1. Introduction

A study of the opening of baled cotton by aerodynamic methods has led to a theoretical investigation of the interactions between fluid flows and fibre tangles. It is hoped thereby to find a gentler process than that presently used to separate the cotton tangles of baled cotton into individual fibres. The present study examines the opening effect on a fibre tangle of an aerodynamic interaction with a dilating airflow.

In a general sense, the theory presented here deals with the fluid flow through a type of porous, deformable, isotropic, solid medium. Little previous work has been published in this area; according to Paria (1963), only two problems in 'isotropic poroviscoelasticity' (i.e. Biot 1955, 1956 and Paria 1958) have been solved, both of which deal with the somewhat remote circumstances associated with settlement in a loaded column of visco-elastic material. In the problem at hand, the porous medium is visualized as a tangle of fibres, having a certain randomness and isotropy associated with its properties, and which undergoes deformation by first stressing the individual fibres and then, as the loads increase in tension, either by a slippage at crossings of fibres or by fibre breakage. One must consider an element of this material containing a large number of fibres and fibre crossings so that it is possible to replace the individual nature of the fibres by a continuum having the properties of a large tangle. In the interest of simplicity, this continuum is assumed to be isotropic. In some respects this medium is like an ordinary fluid; however, this continuum contains voids through which an actual fluid may flow and, at a generic point, additional forces act which are due to the deformation of the tangle and the drag of the fluid flowing through the interstices of the tangle on the elements of that material. The interactions between the fluid and the porous medium are due to their relative

motion; the corresponding interaction force may be described by a modified form of Darcy's law (see, for example, Streeter 1961).

The forces developed within the fibre elements of the tangle are assumed to be a function of the strain and the inter-fibre friction. This, as yet, undetermined function should have the following properties. The upper limit of the stress is determined by the inter-fibre friction; the low-strain portion is determined by an elastic stress–strain relation; there is a smooth transition between elastic stress–strain behaviour and the plastic stress–strain behaviour exhibited when the maximum stress is reached; the compressive stress–strain behaviour is entirely elastic. The smooth behaviour of the stress–strain relation is plausible since, in the neighbourhood of a point within a tangle, not all fibres will be evenly loaded, some having tensions great enough to cause slippage at the interstices of the tangle and others, not as highly loaded, having the capability of straightening and twisting or untwisting (i.e. storing energy elastically). A simple functional representation of the stress–strain behaviour of the fibre tangle will be chosen for the analysis. Due to a lack of experimental data, at this stage in the development of the theory, unknown constants appear in the formulation.

The operation of a dilation chamber consists of alternately pressurizing and depressurizing a symmetric chamber by means of an electrically controlled solenoid valve. The fibre sample is placed at the centre of the chamber so that there is no tendency for the mass centre to move; then, the alternating, symmetrical, dilation and contraction flows act on the sample to pull it apart or crush it. The possibility of slippage between fibres introduces a mechanism for gradually pulling apart the sample after repeated cycling of the chamber. A dilation chamber was fabricated as part of a related experimental programme; however, it was operated prior to the present investigation and was not designed to give information useful for comparison with the analysis presented here.

In the next sections, the derivation of the equations of motion is sketched and the boundary relations at the edges of the fibre sample given. Following this, a discussion of the assumed stress–strain law is presented and the relation of the permeability and lithology factors in the modified Darcy law to the tangle properties are derived. Then, a discussion of the solution to the equations by the method of characteristics will be presented, including the novel aspects of computation with five characteristics. Finally, the results of one series of calculations are given and discussed.

2. Analysis—formulation

Consider a sample of fibre tangle within the interstices of which air is entrapped. The proportion of solid matter in the sample is $(1-f)$, where f is the porosity. The tangle may be thought of as a resistive medium in which the air flows, somewhat like a channel on whose surfaces a fluid friction force is acting. Resistance to the air flow represents a force on the solid elements of the tangle which may cause relative displacements of the fibres and, thus, bring inter-fibre forces into play. The conservation equations for the fluid component are written under the assumption of isotropy for the tangle properties. Also, it is assumed that the

viscous stresses act only on the fibre surfaces internal to the control volume, being negligible within the mass of the fluid itself.

Conservation of fluid mass†

$$\frac{\partial}{\partial t}(f\rho_f)+\nabla.(f\rho_f\mathbf{v}_f)=0. \tag{1}$$

Conservation of fluid momentum

$$f\rho_f\left[\frac{\partial}{\partial t}(\mathbf{v}_f)+\mathbf{v}_f.\nabla\mathbf{v}_f\right]=-\nabla fp+p\nabla f+f\boldsymbol{\tau}.\mathbf{I}, \tag{2a}$$

where $\boldsymbol{\tau}$ is the viscous stress and acts only at the fibre surface, $\mathbf{I}$ is the unit dyadic, p is the fluid pressure, and ρ_f and $\mathbf{v}_f$ are the fluid density and velocity, respectively. In the case of flow through a porous medium, however, the last term in the above equation can be replaced by the modified Darcy law:

$$-\kappa^{-1}\mu f^2(\mathbf{v}_f-\mathbf{v}_s)(1+\mu^{-1}\ell_f d\rho_f|\mathbf{v}_f-\mathbf{v}_s|);$$

$\mathbf{v}_s$ is the velocity of the fibre component of the tangle, κ is the tangle permeability and ℓ_f is a lithology factor which extends the Darcy law validity for relative Reynolds numbers, $\rho_f d|\mathbf{v}_f-\mathbf{v}_s|/\mu$, above the slow-flow regime. Thus ℓ_f represents the inertial effects due to the tortuosity of the streamlines through the porous tangle; d and μ are the fibre diameter and fluid viscosity, respectively. The second term on the right-hand side of equation (2*a*) is the contribution of the pressure forces on the internal fluid–fibre boundaries to the momentum balance. For steady flow and small velocities, the momentum equation reduces to the familiar form

$$-\nabla p=\mu f\kappa^{-1}(\mathbf{v}_f-\mathbf{v}_s).$$

The momentum equation may now be written as

$$f\rho_f\left[\frac{\partial}{\partial t}(\mathbf{v}_f)+\mathbf{v}_f.\nabla\mathbf{v}_f\right]=-f\nabla p-\frac{\mu f^2}{\kappa}(\mathbf{v}_f-\mathbf{v}_s)\left(1+\frac{\ell_f d\rho_f}{\mu}|\mathbf{v}_f-\mathbf{v}_s|\right). \tag{2b}$$

Conservation of fluid energy

The energy equation is written for a fluid in which the viscous effects are negligible, except at the solid–fluid boundaries. Thus,

$$\frac{\partial}{\partial t}(f\rho_f e_f^0)+\nabla.(f\rho_f e_f^0\mathbf{v}_f)=-\nabla.(fp\mathbf{v}_f)+p\mathbf{v}_s.\nabla f$$
$$-\mathbf{v}_s.(\mathbf{v}_f-\mathbf{v}_s)\frac{\mu f^2}{\kappa}\left(1+\frac{\ell_f d\rho_f}{\mu}|\mathbf{v}_f-\mathbf{v}_s|\right), \tag{3a}$$

where $e_f^0=e_f+\frac{1}{2}\mathbf{v}_f^2$ is the total fluid energy. Introducing the perfect gas equation of state and using the mass and momentum conservation equations, the energy equation may be written as

$$f\rho_f\left[\frac{\partial}{\partial t}\left(\frac{\gamma}{\gamma-1}\frac{p}{\rho_f}\right)+\mathbf{v}_f.\nabla\left(\frac{\gamma}{\gamma-1}\frac{p}{\rho_f}\right)\right]=\frac{\partial}{\partial t}(fp)+f\mathbf{v}_f.\nabla p+p\mathbf{v}_s.\nabla f$$
$$+\frac{\mu f^2}{\kappa}(\mathbf{v}_f-\mathbf{v}_s)^2\left(1+\frac{\ell_f d\rho_f}{\mu}|\mathbf{v}_f-\mathbf{v}_s|\right). \tag{3b}$$

† The followng notation is being used: a, scalar quantities; $\mathbf{a}$, vector quantities; $\mathbf{a}$, dyadic tensor quantities.

Conservation of solid mass

The fibre material is assumed to be incompressible; however, since the elements of the tangle may bend and twist, the tangle may compress or expand, thereby occupying more or less of an elemental volume. These changes are reflected in the behaviour of f, which is 1 when no fibres are present in the elemental volume and 0 when no voids are present. Thus, the following mass conservation equation does not contain the fibre material density, ρ_s:

$$\frac{\partial}{\partial t}(1-f)+\nabla.[(1-f)\,\mathbf{v}_s] = 0. \tag{4}$$

Conservation of solid momentum

On the external surface of the control volume, the fibre component occupies the proportion $(1-f)$ of the surface. The control surface must necessarily cut through fibres, on whose cut surfaces fibre stresses act. It should be noted, however, that the internal stress within the fibres is in equilibrium with the hydrostatic pressure applied on the exposed surfaces of the fibres (i.e. those external surfaces of a fibre that are not in contact with another fibre) and the stress transmitted from fibre to fibre across the fibre contact areas. It is this latter portion of the fibre stress, due to inter-fibre forces and associated with bending and twisting of the fibres, which is directly responsible for tangle strains.

In the present model, the splitting of the internal fibre stress into hydrostatic and inter-fibre force components is justified by the isotropic nature of the stresses set up in the individual fibres by their immersion in the fluid and the relatively large elastic modulus of the fibre material; that is, the hydrostatic forces uniformly crush the fibre material, which, however, undergoes insignificant deformations that are not of the kind responsible for gross tangle strains, i.e. twisting and bending (although it is conceivable that, at sufficiently high hydrostatic pressure levels, the fibres will buckle, they are generally twisted and bent in their natural state, being therefore quite resistant to such deformations. It should be noted that other porous deformable media whose elements are not fibres and whose material is much more compliant will not satisfy the assumptions of the present stress model). Since the hydrostatic portion of the fibre stress is a consequence of the fibre surfaces being exposed to fluid pressure, it follows that any reduction in exposed surface area, as, for example, by mutual fibre contact, would reduce that stress component. This hydrostatic stress in a given direction would, as usual, be given by the fluid pressure multiplied by the projection of the exposed surface area in that direction. In the absence of any pertinent data, it is convenient to assume that the reduction in exposed area for a fibre is linear in the number density of fibres of $(1-f)$ and that, therefore, for an isotropic tangle, the hydrostatic forces within the fibres at the surface of the control volume is given by $p(1-f)[1-c(1-f)]$, where c is a constant which depends on the type of fibre in the tangle.

With the help of the solid mass conservation equation the momentum equation may be written as

$$\rho_s(1-f)\left[\frac{\partial}{\partial t}(\mathbf{v}_s)+\mathbf{v}_s.\nabla\mathbf{v}_s\right] = -p\nabla f-\nabla[(1-f)(1-c(1-f))\,p]+\nabla.\boldsymbol{\varpi} + \frac{\mu f^2}{\kappa}(\mathbf{v}_f-\mathbf{v}_s)\left(1+\frac{\ell_f\, d\rho_f}{\mu}|\mathbf{v}_f-\mathbf{v}_s|\right), \quad (5a)$$

or, combining the first two terms of the right-hand side,

$$\rho_s(1-f)\left[\frac{\partial}{\partial t}(\mathbf{v}_s)+\mathbf{v}_s.\nabla\mathbf{v}_s\right] = -2cp(1-f)\nabla f-(1-f)(1-c(1-f))\,\nabla p + \nabla.\boldsymbol{\varpi}+\frac{\mu f^2}{\kappa}(\mathbf{v}_f-\mathbf{v}_s)\left(1+\frac{\ell_f\, d\rho_f}{\mu}|\mathbf{v}_f-\mathbf{v}_s|\right). \quad (5b)$$

The last term represents the fluid drag upon the tangle and is equal, but opposite in direction, to the resistance encountered by the fluid. The $\boldsymbol{\varpi}$ term is a stress tensor acting on the control surfaces due to deformations of the tangle and is a function of the porosity, the normal forces between fibres at crossings within the tangle and the ability to store energy by deforming the individual fibres. This function will be dealt with at length in a following section. It should be noted that, in a dilation flow, no shear stress terms will appear in $\boldsymbol{\varpi}$ because of the symmetry of the geometry and of the forces.

Conservation of solid energy

Since the fibres are considered to be incapable of interchanging heat energy with the fluid and the thermodynamic state of the fibres is of no interest, there is no necessity for writing an energy equation; such an equation would not be independent, but just the scalar product of the velocity vector, $\mathbf{v}_s$, with the just previously derived momentum equation.

Stress–strain relation

Consider the situation where one attempts to exert the maximum tension on a surface of the control volume. In this case, the fibres passing through the surface would be under the maximum tension consistent with the onset of slippage between the fibres in a tangle. It is assumed that this stress level is fixed by inter-fibre friction so that the maximum tensile stress is proportional to the number density of fibres, n_s, the maximum force, F, required to withdraw a single fibre in contact with other fibres and a characteristic length, ℓ, which is of the order of a fibre diameter.

There is some disagreement about the dependence of the frictional force upon the normal force between fibres, N, and contact area, but for parallel fibres Grálen & Olafsson (1947), DuBois (1959) and Postle, Ingham & Cox (1952) agree on the form

$$F = a+bN,$$

where a and b are functions of the average fibre diameter, variability and the surface friction coefficient. In the present case, F is normal to the control surface

and N is the result of stress within the tangle. It seems reasonable to take N as being proportional to stress within the tangle, which, in turn, is the result of stressing the fibres at the control surfaces. N is therefore taken as being proportional to F, so that

$$F = a + b\hat{c}F \rightarrow F = a/(1 - b\hat{c}).$$

Since $n_s = \rho_s(1-f)/m_s$, where ρ_s is the density of the fibre material, m_s is the average mass of a length of fibre contained within a control volume of unit dimensions, and one may combine all the unknown constants into a single quantity, α, which must be experimentally determined, it is possible to write the following expression for the maximum tensile stress, $\tilde{\omega}'$:

$$\tilde{\omega}' = 2(1-f)\rho_s\alpha,$$

where

$$\alpha = \frac{1}{2}\frac{\ell}{m_s}\left(\frac{a}{1-b\hat{c}}\right).$$

When the strain is small, however, the tangle acts like an elastic material in which energy is stored by distorting the elements of the tangle. In tension, as the stress increases, the tangle undergoes small adjustments in the form of slippages at fibre crossings until the loading reaches $\tilde{\omega}'$, at which point slippage occurs with no further increase in loading. As stated in §1, it is supposed that the transition between these two behaviours (elastic–plastic) is a smooth one, so that in tension the interfibre forces are assumed to be given by $\tilde{\omega} = \tilde{\omega}' \operatorname{erf} k\sigma$, where σ is the strain, k is an undetermined constant and erf denotes the error function. The error function has been picked because of the relative simplicity with which it satisfies the elastic–plastic transition requirement. At this time, there are no other grounds on which to base a choice.

In compression, the maximum loading would be the crushing load, and slippage between fibres would not be an important factor; energy would be stored in the tangle by bending or twisting of the fibres. It has been observed by the author that it requires much more force to permanently deform a wad of, for instance, surgical cotton by compressing it rather than by pulling it apart. Since it is not anticipated that such compressive loads will be generated in a dilation chamber (indeed, this would be self defeating), it will be supposed for present purposes that the tangle is linearly elastic in compression. Moreover, because bending and twisting are the modes of distorting the tangle under low tensile loads, it is supposed that the stress–strain behaviour is continuous at the zero stress level. Also, it is supposed that, when relaxing from a tensile load, a linear elastic, stress–strain behaviour is followed since slippage cannot be reversed and was assumed to account for the non-linearities in the stress–strain relation. (It is realized that for some fibres, such as wool, which may have much higher interfibre friction, slippage may occur at large strains where non-linear bending and twisting of fibres can be important.) A permanent set will be put into the tangle after a substantial tensile strain. Inclusion of other effects, such as a time-dependent recovery response in the stress–strain relation, cannot at this time be justified by any observations known to the author.

The basic assumptions underlying the stress–strain relations are those of elastic behaviour of the individual fibres and the occurrence of irreversible slip

between elements of the tangle. The latter has been assumed, on the basis of personal observation and in the interest of simplicity, to be dependent only on the normal force between fibres (and, ultimately, on the stress level within the tangle) and not a function of the relative velocity between the fibres or subject to a stick–slip effect due to substantial differences in static and kinetic friction forces; this is in agreement with the experiments of Lord (1955*a*) and Grålen & Olafsson (1947) on cotton and wool, although some man-made fibres are found to exhibit stick–slip behaviour. Hence, as illustrated in figure 1,

$$\begin{aligned} \tilde{\omega} &= \tilde{\omega}' \operatorname{erf}(k(\sigma-\sigma_*)) \quad \text{for } \sigma-\sigma_* \geqslant 0 \text{ and increasing,} \\ \tilde{\omega} &= 2k\pi^{-\frac{1}{2}}\tilde{\omega}'(\sigma-\sigma_*) \quad \text{for } \sigma-\sigma_* < 0 \text{ or decreasing,} \end{aligned} \tag{6}$$

where σ_* is obtained from solution of the following algebraic equation whenever σ starts to decrease:

$$k(\sigma-\sigma_*) = \tfrac{1}{2}\pi^{\frac{1}{2}} \operatorname{erf}(k(\sigma-\sigma_*)). \tag{7}$$

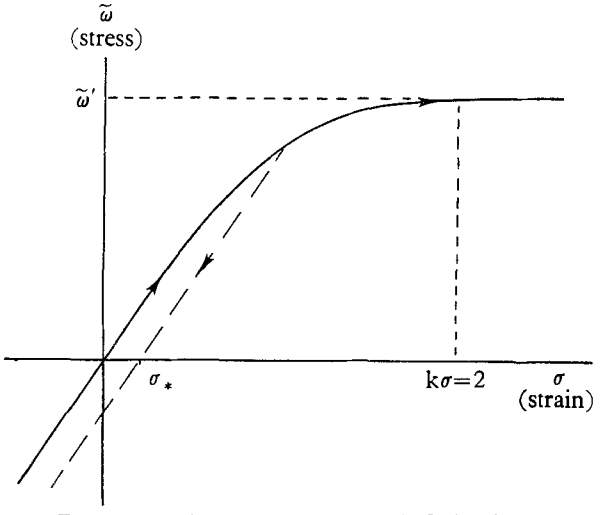

FIGURE 1. Assumed stress–strain behaviour.

The strain, σ, may be related to the divergence rate of fibre tangle. Consider a moving element, always composed of the same fibres; then, using the solid mass conservation equation,

$$\sigma-\sigma_0 = \int_{t_0}^{t} dt \nabla . \mathbf{v}_s = -\log\left(\frac{1-f}{1-f_0}\right),$$

where the subscript 0 denotes conditions at $t = t_0$ along a solid (fibre) particle or world line in the flow of fibre and fluid. Thus,

$$\nabla\tilde{\omega} = \left(\frac{\partial\tilde{\omega}}{\partial f} + \frac{1}{1-f}\frac{\partial\tilde{\omega}}{\partial\sigma}\right)\nabla f \equiv \frac{d\tilde{\omega}}{df}\nabla f. \tag{8}$$

Because of the requirement of knowing σ_*, one must compute this quantity along the solid particle path through the point of interest. In a characteristics method of solution, this is equivalent to having an additional, implicit, characteristic direction.

In the light of the above discussion, the conservation of momentum equation for the solid fraction, without shearing forces, may be written as

$$\rho_s(1-f)\left[\frac{\partial}{\partial t}(\mathbf{v}_s)+\mathbf{v}_s.\nabla\mathbf{v}_s\right]=\left[\frac{d\tilde{\omega}}{df}-2pc(1-f)\right]\nabla f-(1-f)(1-c(1-f))\nabla p$$
$$+\frac{\mu f^2}{\kappa}(\mathbf{v}_f-\mathbf{v}_s)\left(1+\frac{\ell_f d\rho_f}{\mu}|\mathbf{v}_f-\mathbf{v}_s|\right). \qquad (5c)$$

Permeability and lithology factor

The modified Darcy law (i.e. Tek–Darcy, cf. Streeter 1961) contains two coefficients, κ and ℓ_f, which are functions of the porous medium through which a fluid flows. Lord (1955*b*) has experimentally determined the permeability, κ, for air flow through plugs of textile fibres as a function of the porosity and type of fibre in the sample. He found that the data were well represented by the expression

$$\kappa = 0{\cdot}903d^2f^5/(16(1-f)^\beta), \qquad (9a)$$

where $\beta = 1{\cdot}391$ for cotton and d is the effective fibre diameter based upon the specific surface, i.e. surface area per unit volume of fibre. It should be noted, however, that the maximum Reynolds number (based upon fibre diameter) in these experiments was about 0·1; for Reynolds numbers above this range the additional term in the modified Darcy law becomes of importance. In the present instance, maximum Reynolds numbers of about 30 are anticipated, so that an estimate of the lithology factor is desirable.

No universal dependence of the lithology factor, ℓ_f, upon the porosity characteristics has been found in the literature. However, there does exist a body of data for the pressure drop through woven grids at Reynolds numbers of present interest. Although the approximation of a tangle by a woven grid is not rigorous, it is possible, by identifying the porosity with the ratio of open volume to total volume of a grid whose elements are circular cylinders, and the distance over which the pressure gradient acts with the fibre diameter divided by the solidity, to derive a pressure drop law with a low-order term in reasonable agreement with the results of Lord (1955*b*) and from which an expression for the lithology factor may be extracted. Following Elder (1959), a simplified version of the experimental law found by Davis (1957) for the pressure drop through a grid is used. Rearranging this law and identifying it with the modified Darcy law, it is found that

$$\kappa = f^2d^2/[44(1-f^2)(1-f)], \qquad (9b)$$

$$\ell_f = (1-f^2)/88f^5. \qquad (10)$$

By using (10) for ℓ_f along with (9*a*) for κ, it is supposed that the higher-order correction to the actual slow-flow behaviour is, at least, approximately described.

Edge conditions

In many problems, including the one of interest, at the edge of the fibre sample, one can identify an interface separating the gas–fibre mixture and the surrounding gas. In the present approximation, this interface is a boundary which no fibres can cross. Considering a control volume which always contains the bound-

ary and has vanishing thickness in the direction normal to the boundary, one can write the conservation equations in the co-ordinate system moving with the boundary as

$$\rho_{f_0}\bar{v}_{fn_0} = f_1\rho_{f_1}\bar{v}_{fn_1} = \dot{m}, \tag{11a}$$

$$\rho_{f_0}\bar{v}^2_{fn_0} + f_1 p_0 = f_1(\rho_{f_1}\bar{v}^2_{fn_1} + p_1), \tag{11b}$$

$$\left[\frac{\gamma}{\gamma-1}\frac{p}{\rho_f} + \tfrac{1}{2}\bar{v}_f^2\right]_0 = \left[\frac{\gamma}{\gamma-1}\frac{\gamma}{\gamma-1}\frac{p}{\rho_f} + \tfrac{1}{2}\bar{v}_f^2\right]_1, \tag{11c}$$

$$\bar{v}_{s_n} = 0, \quad p_0(1-f_1) = p_1(1-f_1) - \tilde{\omega}_{1_n} - cp_1(1-f_1)^2, \tag{11d, e}$$

where the velocities in these moving co-ordinates are denoted by a superscript $-$, their components normal to the boundary surface are denoted by subscript n, and conditions inside and outside the gas–fibre mixture are denoted by subscripts 1 and 0, respectively. It will be seen, subsequently, that the above conditions are analogous to the jump conditions across a shock wave in a single gas. Non-trivial solutions have been worked out only for the one-dimensional case and will be given in the following sections.

One-dimensional unsteady flow equations

The governing equations derived in the previous sections will be applied to the description of the phenomena inside a symmetrical, one-dimensional, dilation chamber in which the fibre sample is located at the centre. There are no shearing terms present in this situation, so that the equations (1)–(5) reduce to:

conservation of solid mass:

$$\partial f/\partial t + v_s(\partial f/\partial r) - (1-f)(\partial v_s/\partial r) = 0; \tag{12}$$

conservation of fluid mass:

$$(\partial/\partial t)(f\rho_f) + v_f(\partial/\partial r)(f\rho_f) + f\rho_f(\partial v_f/\partial r) = 0; \tag{13}$$

conservation of solid momentum:

$$\rho_s(1-f)[(\partial v_s/\partial t) + v_s(\partial v_s/\partial r)] - \rho_s a_s^2(\partial f/\partial r) + (1-f)c'(\partial p/\partial r) = \mu f^2\kappa^{-1}(v_f - v_s)I, \tag{14}$$

where

$$a_s^2 = \rho_s^{-1}[(d\tilde{\omega}/df) - 2c(1-f)p], \quad c' = 1 - c(1-f), \quad I = 1 + \ell_f d\rho_f\mu^{-1}|v_f - v_s|;$$

conservation of fluid momentum:

$$f\rho_f[(\partial v_f/\partial t) + v_f(\partial v_f/\partial r)] + f(\partial p/\partial r) = -\mu f^2\kappa^{-1}(v_f - v_s)I; \tag{15}$$

conservation of fluid energy:

$$\frac{f}{\gamma-1}\left[\left(\frac{\partial p}{\partial t} - \frac{\gamma p}{\rho_f}\frac{\partial \rho_f}{\partial t}\right) + v_f\left(\frac{\partial p}{\partial r} - \frac{\gamma p}{\rho_f}\frac{\partial \rho_f}{\partial r}\right)\right] - p\frac{\partial f}{\partial t} - pv_s\frac{\partial f}{\partial r} = \frac{\mu f^2}{\kappa}(v_f - v_s)^2 I. \tag{16}$$

One-dimensional edge conditions

Equations (11) reduce to:

$$\rho_{f_0}\bar{v}_{f_0} = f_1\rho_{f_1}\bar{v}_{f_1} = \dot{m}, \tag{17a}$$

$$\rho_{f_0}\bar{v}^2_{f_0} + f_1 p_0 = f_1(\rho_{f_1}\bar{v}^2_{f_1} + p_1), \tag{17b}$$

$$\left(\frac{\gamma}{\gamma-1}\frac{p}{\rho_f} + \tfrac{1}{2}\bar{v}_f^2\right)_0 = \left(\frac{\gamma}{\gamma-1}\frac{p}{\rho_f} + \tfrac{1}{2}\bar{v}_f^2\right)_1, \tag{17c}$$

$$p_0(1-f_1) = p_1(1-f_1) - \tilde{\omega}_1 - cp_1(1-f_1)^2, \tag{17d}$$

where $\bar{v} = v - v_s$ and subscripts 0 and 1 denote conditions just outside and inside the fibre boundary, respectively. The non-trivial solutions are derived in a fashion similar to that used for the ordinary gasdynamic equations. The resulting jump conditions are

$$p_1/p_0 = \tfrac{1}{2}(1-\delta^2) + \tfrac{1}{2}(1+\delta^2)(M_0^2/f_1) \pm \tfrac{1}{2}([(1-\delta^2)+(1+\delta^2)(M_0^2/f_1)]^2 - 4[(1+\delta^2)(M_0^2/f_1^2)\{1+2\delta^2(1-\delta^2)^{-1}(1-f_1)\}-\delta^2])^{\frac{1}{2}}, \quad (18a)$$

or

$$p_0/p_1 = \tfrac{1}{2}[1+\delta^2(1-f_1)]^{-1}[1+\delta^2(1-f_1)-\delta^2 f_1+(1+\delta^2)M_1^2\{1+2\delta^2(1-\delta^2)^{-1}(1-f_1)\} \pm ([1+\delta^2(1-f_1)-\delta^2 f_1+(1+\delta^2)M_1^2\{1+2\delta^2(1-\delta^2)^{-1}(1-f_1)\}]^2 - 4f_1[1+\delta^2(1-f_1)][(1+\delta^2)M_1^2-\delta^2])^{\frac{1}{2}}], \quad (18b)$$

$$\rho_{f_1}/\rho_{f_0} = \tfrac{1}{2}[1+\delta^2(1-\delta^2)^{-1}M_0^2]^{-1}[1+(1+\delta^2)(1-\delta^2)^{-1}(M_0^2/f_1) \pm ([1+(1+\delta^2)(1-\delta^2)^{-1}(M_0^2/f_1)]^2 - 4(1-\delta^2)^{-1}(M_0^2/f_1^2)[1+\delta^2(1-\delta^2)^{-1}M_0^2])^{\frac{1}{2}}], \quad (19a)$$

or

$$\rho_{f_0}/\rho_{f_1} = \tfrac{1}{2}[1+\delta^2(1-\delta^2)^{-1}M_1^2]^{-1}[1+(1+\delta^2)(1-\delta^2)^{-1}M_1^2 \pm ([1+(1+\delta^2)(1-\delta^2)^{-1}M_1^2]^2 - 4f_1(1-\delta^2)^{-1}M_1^2[1+\delta^2(1-f_1)] \times [1+\delta^2(1-\delta^2)^{-1}M_1^2])^{\frac{1}{2}}]. \quad (19b)$$

In each of the above equations, the positive square root sign gives the jump conditions provided M_0 or M_1 is the relative Mach number, $\bar{v}_f/a_f$, of the flow entering the boundary, while the negative sign gives the conditions when M_0 or M_1 is the relative Mach number of the flow leaving the boundary.

The desired velocity ratio results are obtained by use of the mass conservation equation (17*a*) and either of equations (19*a*) or (19*b*). Thus,

$$v_{f_1}/v_{f_0} = [f_1 \times \text{equation (19}a\text{)}]^{-1} \quad \text{or} \quad v_{f_0}/v_{f_1} = [f_1/\text{equation (19}b\text{)}]. \quad (20a, b)$$

Similarly, by using (17*d*) and either (18*a*) or (18*b*), relations for $\tilde{\omega}_1$ may be derived in terms of f_1 and conditions on one side or the other of the boundary.

3. Characteristics solution

Characteristic directions

The one-dimensional unsteady flow equations developed in the previous section can be shown to possess five explicit characteristic directions. The details of finding the characteristic directions and the corresponding compatibility relations need not be reproduced here because of the rather routine nature of the manipulations; they are available in the appendix of Taub (1965). The characteristic directions are found to be the solutions of the following equation for dr/dt

$$[(dr/dt)-v_f]\{(-a_s^2+[(dr/dt)-v_s]^2)(a_f^2-[(dr/dt)-v_f]^2)+(1-f)c'(\rho_f a_f^2/f\rho_s) \times [(dr/dt)-v_f]([(dr/dt)-v_f]+(\gamma-1)\gamma^{-1}[(dr/dt)-v_s])\} = 0, \quad (21)$$

where $c' = 1-c(1-f)$. It is seen that there are five characteristic directions; one of these is immediately identified as the fluid trajectory while the others can be shown, for cases of interest, to be close to the usual fluid characteristics (i.e.

$dr/dt = v_f \pm a_f$) and the analogous elastic body characteristics (i.e. $dr/dt = v_f \pm a_s$). This result is not entirely unexpected since the interaction will be weak if the air is not too impeded. The fluid trajectory characteristic is found to be present in fluid flows when there is a means of entropy production, which, in this case, is due to the resistance of the tangle to the fluid flow.

Equation (21) may be solved numerically by means of a digital computer or by use of a tedious analytical procedure; however, one may take advantage of the closeness of the characteristic directions to that for fluids and elastic bodies (since $(1-f)\,c'(\rho_f/f\rho_s) \ll 1$ in cases of interest) to derive a set of first-order estimates for the differences between these directions and the characteristic directions. In order to do this, (21) is cast into the following form:

$$\{-(a_s+g)^2+[x-(v_s+h)]^2\}\{(a_f+i)^2-[x-(v_f+j)]^2\} = 0. \tag{22}$$

Expanding this into powers of $x \equiv dr/dt$ and comparing this with a similar expansion of (21), a set of non-linear equations may be derived which can be linearized by assuming that $i \ll a_f$ and $j \ll a_f$ or v_f. The resulting equations for g, h, i, j are

$$\left.\begin{aligned} j &= -h, \\ (2a_f)\,i + 2(v_s-v_f)\,h + (2a_s)\,g &= \bar{c}(1-\bar{d}), \\ (4v_sa_f)\,i + 2(v_s^2-a_s^2+a_f^2-v_f^2)\,h + (4v_fa_s)\,g &= \bar{c}[2v_f-\bar{d}(v_s+v_f)], \\ 2a_f(v_s^2-a_s^2)\,i + 2[v_f(v_s^2-a_s^2)+v_s(a_f^2-v_f^2)]\,h - 2a_s(a_f^2-v_f^2)\,g &= \bar{c}(v_f^2-v_sv_f\bar{d}), \end{aligned}\right\} \tag{23}$$

where $\bar{c} = (1-f)\,c'(\rho_f/f\rho_s)\,a_f^2$ and $\bar{d} = (\gamma-1)/\gamma$. As long as $\bar{c} \ll a_f^2$, it can be shown that the corrections g, h, i, j are small.

Compatibility relations

Along each characteristic, a compatibility relation among differentials of the variables may be written in the form

$$A\,df + B\,d\rho_f + C\,dp + D\,dv_f + E\,dv_s = F'\,dt, \tag{24a}$$

where $A, B, \ldots, F'$ are the following functions:

$$\left.\begin{aligned} A &= p\rho_f(1-f)\,c'[(dr/dt)-v_f]\,(v_f-v_s) - f\rho_f\rho_s(\gamma-1)^{-1}\{a_s^2-[(dr/dt)-v_s]^2\} \\ &\qquad \times\{[(dr/dt)-v_f]^2-a_f^2\} \\ &\quad -f\rho_s\rho_f(\gamma-1)^{-1}[(dr/dt)-v_s]\{(\gamma-1)\,\gamma^{-1}a_f^2[(dr/dt)-v_s]+[(dr/dt)-v_f]^3\}, \\ B &= fp(1-f)\,c'[(dr/dt)-v_f]\{[(dr/dt)-v_s]-\gamma(\gamma-1)^{-1}[(dr/dt)-v_f]\} \\ &\quad -f^2\rho_s(\gamma-1)^{-1}\{a_s^2-[(dr/dt)-v_s]^2\}\{[(dr/dt)-v_f]^2-a_f^2\}, \\ C &= -f(\gamma-1)^{-1}[f\rho_s\{a_s^2-[(dr/dt)-v_s]^2\}-(1-f)\,c'\rho_f\{(dr/dt)-v_f\}^2], \\ D &= f\rho_f[p(1-f)\,c'[(dr/dt)-v_s]-f\rho_s(\gamma-1)^{-1}[(dr/dt)-v_f] \\ &\qquad \times\{a_s^2-[(dr/dt)-v_s]^2\}], \\ E &= \rho_s(1-f)f\rho_f(\gamma-1)^{-1}\{(\gamma-1)\,\gamma^{-1}a_f^2[(dr/dt)-v_s]-[(dr/dt)-v_f]^3\}, \\ F &= -(1-f)\,c'\{p[(dr/dt)-v_s]-\rho_f(v_f-v_s)\,[(dr/dt)-v_f]^2\} \\ &\quad +f\rho_s\{(\gamma-1)^{-1}[(dr/dt)-v_f]-(v_f-v_s)\}\{a_s^2-[(dr/dt)-v_s]^2\} \\ &\quad +f\rho_f(\gamma-1)^{-1}\{(\gamma-1)\,\gamma^{-1}a_f^2[(dr/dt)-v_s]-[(dr/dt)-v_f]^3\}, \\ F' &= F[\mu f^2\kappa^{-1}(v_f-v_s)\,I], \end{aligned}\right\} \tag{25}$$

dr/dt is a characteristic direction obtained from solution of (21).

Along a given characteristic, (24*a*) may be changed into a difference equation by means of an appropriate approximation. In the present study, the simple relations, $df = f_{II} - f_I$, $d\rho_f = \rho_{f_{II}} - \rho_{f_I}$, etc. were used, where I and II denote conditions at the initial and final points along a length of the characteristic curve. Identifying subscript II with a point (r, t) at which it is desired to find the solution, the equation may be rearranged to be

$$Af_{II} + B\rho_{f_{II}} + Cp_{II} + Dv_{f_{II}} + Ev_{s_{II}} = F'\,dt + Af_I + B\rho_{f_I} + Cp_I + Dv_{f_I} + Ev_{s_I}; \quad (24b)$$

here dt is the time increment along the characteristic curve.

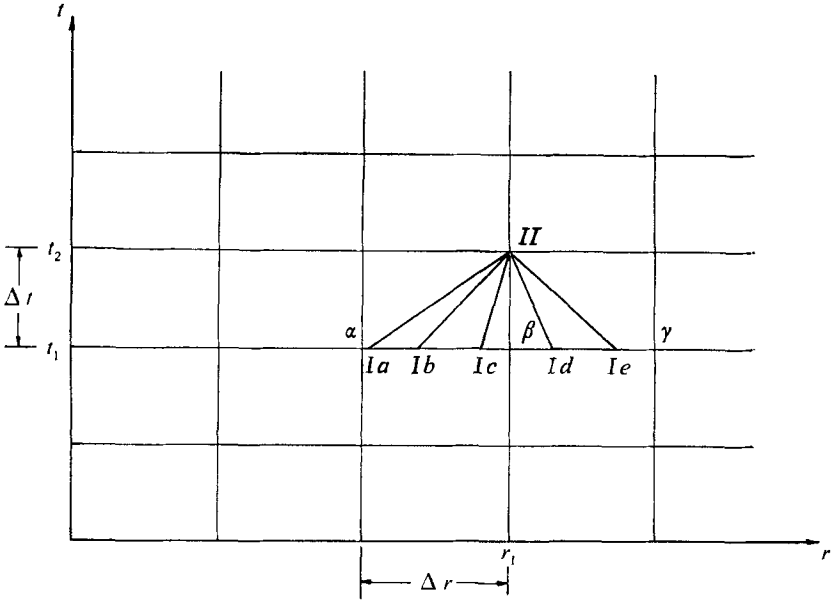

FIGURE 2. Characteristics at an interior point.

Solution procedure—interior point

Because of the multiplicity of characteristic directions and their dependence upon the solution, the following iteration procedure is used. If one supposes that at a point all five characteristic directions are known, then a system of linear equations can be written for the dependent variables, with subscript II denoting conditions at the common end-point of the characteristic curves passing through that point and with subscript $I_a, I_b, \ldots, I_e$ denoting conditions at the initial point of each characteristic, respectively. This is illustrated in figure 2, in which a grid in (r, t) is laid out with equal increments Δr, and with Δt chosen so that points $I_a \ldots I_e$ lie between points α and γ.

The solution is presumed known for all grid points along $t = t_1$ and it is desired to find the solution at point II. In order to start the calculation one must either estimate or guess at the solution so that the characteristic directions at point II may be computed. A simple first estimate for the solution at (r_1, t_2) is obtained by using the solution at (r_1, t_1) (i.e. point β). Then characteristic curves may be constructed by going towards the previous time, t_1, along a straight line whose

slope has the characteristic direction until it passes through time t_1 at the point I_a, I_b,... or I_e. The values of the dependent variables at these last-mentioned points are found by interpolation between their values at points α, β and γ. When computing the values of the coefficients $A, B, \ldots, F'$ the values of the dependent variables used are taken as the average between their values at I and II. Also, the average characteristic direction along the characteristic curve is used to find points $I_a \ldots I_e$.

When using the above procedure, the five equations of the same type as (25) result and are then solved as a set of linear equations for the dependent variables at point II. Then using the averaging technique, the calculation is repeated until the solution at point II no longer changes. The iteration procedure has been found to converge, provided that the $F'\,dt$ terms are not too large; the upper limit for dt is determined by the convergence requirement.

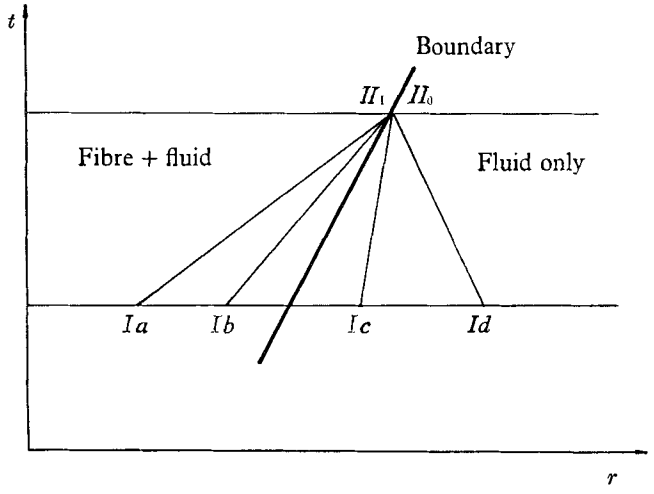

FIGURE 3. Characteristics at the fibre boundary.

Solution procedure—fibre boundary

In the present analysis, the solution is discontinuous across the fibre boundary and its calculation requires special attention. The boundary point is treated as a dual point, each lying infinitesimal distances on either side of the discontinuity, with the jump conditions, equations (18)–(20), specifying the relations between the solutions. The situation is that shown in figure 3.

Outside the boundary, only fluid is found; therefore only the usual compressible fluid characteristics are applicable and at most two characteristics can intersect the boundary point II_0 from points outside the boundary. However one of these, namely the fluid particle paths, may lie within the fibre boundary and in this case would be counted among the characteristics approaching the boundary point II_1 from within the fibre boundary. It is possible for a maximum of three characteristics to pass through the boundary point II_1. One of these has just been mentioned, while of the other two characteristics, one has a direction close to $v_f \pm a_f$ and the other has direction close to $v_s \pm a_s$. Thus, the characteristics passing through the boundary give rise to four compatibility relations in the

form of (24), while the jump conditions give three equations for the eight quantities f_1, ρ_{f_0}, ρ_{f_1}, p_0, p_1, v_{f_0}, v_{f_1} and v_{s_1}. The additional equation necessary to complete the formulation is obtained by use of the solid mass conservation equation at the boundary, viz.

$$df_1/dt = (1-f_1)\nabla . \mathbf{v}_s. \tag{26}$$

In order to evaluate the divergence term, the net point just within the fibre boundary is used. Hence the dual boundary point and the adjacent net point are to be solved simultaneously. In practice one first uses the solution at the previous time to evaluate $\nabla . \mathbf{v}_s$, then solves the system of equations for the dual boundary point, computes the solution at the adjacent inside net point, re-estimates $\nabla . \mathbf{v}_s$ and then recomputes the boundary solution. Actual calculation shows that the boundary solution is almost unchanged by the re-estimation of $\nabla . \mathbf{v}_s$.

Application to flow in dilation chamber

In a dilation chamber, the fibre sample is situated so that its axis of symmetry coincides with the axis of the chamber as shown in figure 4. Thus, by enforcing the symmetry conditions, $v_f = v_s = 0$, at the axis, only half of the problem need be considered. Further, outside the fibre boundary, where only fluid is present, it is profitable to use ordinary compressible fluid characteristics methods for non-constant entropy flows.

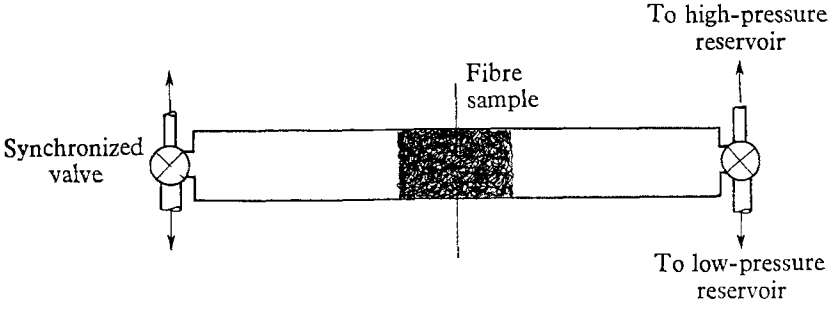

FIGURE 4. Schematic diagram of a one-dimensional dilation chamber.

At the ends of the chambers, valves will be present which, it is supposed, will alternately connect the chamber with two pressure reservoirs of infinite extent, and of high and low pressure, respectively. For the present analysis, it is assumed that the valves may be replaced by a condition which specifies the pressure at the end walls as a function of time, namely a square wave which attains one of two values depending upon which phase of the period a given time lies within. Since no fibres are present at the valves, the end-wall conditions are easily calculated from a specification of the pressure and two of the ordinary fluid characteristics, one of which is the fluid trajectory.

At a given initial time, the state of the chamber and its contents are specified; in this instance, the chamber contents are at rest, the fluid pressure and density are uniform and the end-wall valve has just opened to the low-pressure reservoir with a pressure level lower than that within the chamber. The value of fibre contact factor, c, has arbitrarily been chosen to be 10^{-3}, reflecting the smallness

of the effect it describes. The constants in the stress–strain law, α and k, were determined roughly from a simple experiment with weights applied to a suitable sample and the observation of strains; this gave values of 7·1 and 2 for α and k respectively. The fibre material density, ρ_s, was taken to be 96·9 lb./ft.[3]

4. Interaction histories

The major features of the flow are illustrated by a wave diagram of the events of the early time period as shown in figure 5. After the valve opens, an air wave propagates inward from the end wall towards the fibre face and, upon impingement, gives rise to two waves, namely a reflected expansion and a transmitted

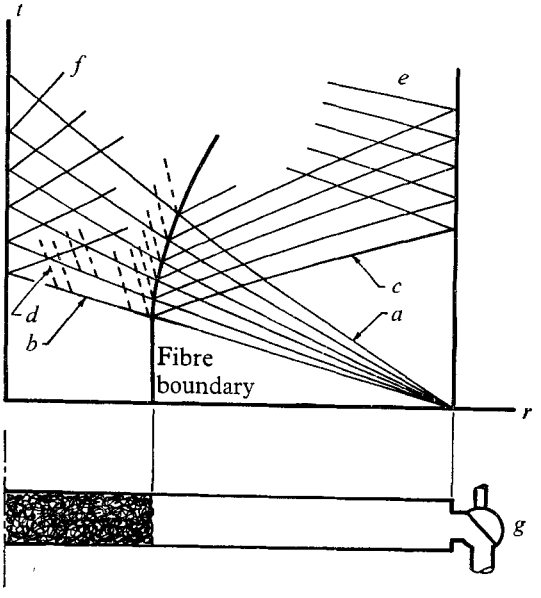

FIGURE 5. Wave diagram for early time period. *a*, initial expansion wave fan; *b*, air expansion waves transmitted through fibre face; *c*, air expansion waves reflected from fibre face as expansion waves; *d*, fibre expansion waves; *e*, air expansion waves reflected at end walls as compression waves; *f*, air expansion waves reflected from axis of symmetry; *g*, valve open to low-pressure reservoir.

expansion wave. The reflected air wave will propagate back out to the end wall, where the constant pressure condition will reflect it inward as a compression wave. The transmitted air wave will continue to propagate inward until the axis of symmetry is reached, where it may be said to reflect as an expansion wave which travels outward until it impinges upon the fibre boundary, where it gives rise to transmitted and reflected waves. It should be recognized that, because the sound speed associated with the elastic properties of the fibre tangle is generally much smaller than the sound speed in air, waves with propagation speeds approximately equal to the fibre tangle's elastic sound speed will originate at every point along a wave propagating through the air contained within the tangle; these waves are termed fibre waves and are analogous to the waves produced in any elastic body which is subjected to a disturbance. After a few reflexions, it becomes impossible to trace the individual waves. Because of the stability

limitation on the permissable step size of the calculation and the cost of large blocks of time on an electronic computer, only a limited time period was covered in the calculations.

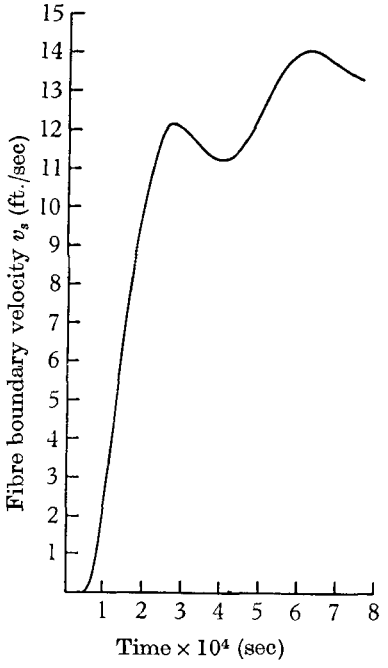

FIGURE 6. Fibre boundary velocity history.

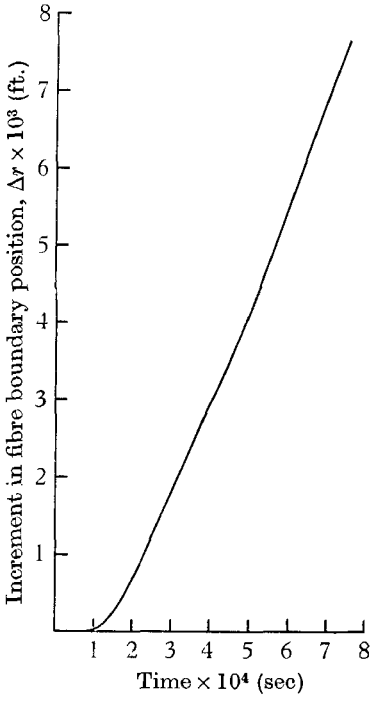

FIGURE 7. History of fibre boundary motion.

The results of a series of calculations are shown in figures 6–11, in which a fibre sample initially of 0·11 ft. length and 0·9 porosity interacts with the flow in a 0·20 ft. dilation chamber. The chamber is at a pressure of $3{\cdot}5 \times 10^3$ lb./ft.^{2} with a fluid density of $3{\cdot}96 \times 10^{-3}$ slugs/ft.^{3} when the end-wall valve is opened to a reservoir with a pressure of $2{\cdot}82 \times 10^3$ lb./ft.^{2}. The solution curves shown in figures 8–11 are separated by approximately equal time intervals of $0{\cdot}72 \times 10^{-4}$ sec with the first curve in each figure corresponding to $0{\cdot}34 \times 10^{-4}$ sec after valve opening.

Because of the viscous interaction taking place between air and fibres, the air waves are attenuated as they pass through the tangle. Thus, for example, the first expansion wave transmitted through the tangle may be so attenuated that its reflexion from the axis of symmetry, or its additional reflexion from the inside of the fibre boundary, will be negligible. The effects of reflexions from the end walls are especially evident in the behaviour of the fibre boundary velocity. As shown in figure 6, a slackening off of this velocity occurs at about $2{\cdot}5 \times 10^{-4}$ sec, which is approximately the time required for an expansion wave to travel from the valve at the end wall to the fibre sample face, reflect to the valve, where it reflects as a compression wave, and to return to the sample face. The similar dip in the fibre face velocity shown in figure 6 at about 6×10^{-4} sec is the result of continued reflexions from the end wall and sample face of the compression waves responsible for the previous slackening off of the fibre boundary velocity.

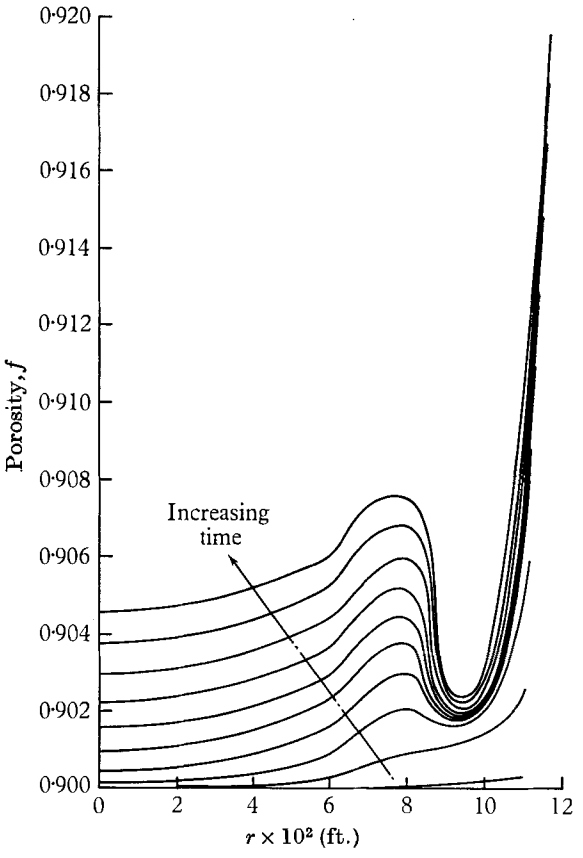

FIGURE 8. History of fibre porosity distribution.

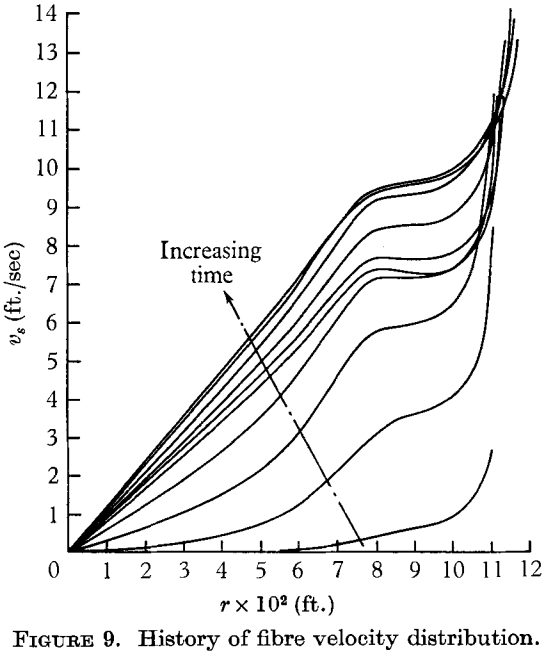

FIGURE 9. History of fibre velocity distribution.

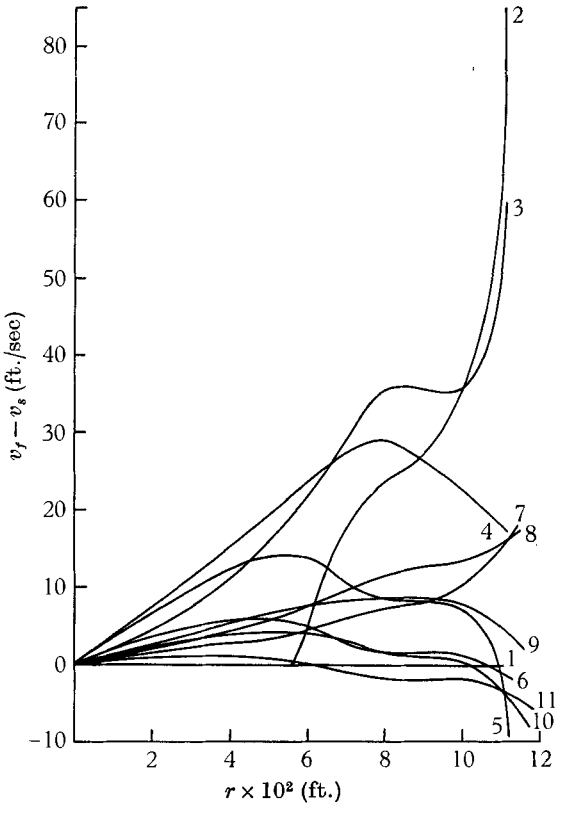

FIGURE 10. History of velocity difference distribution.

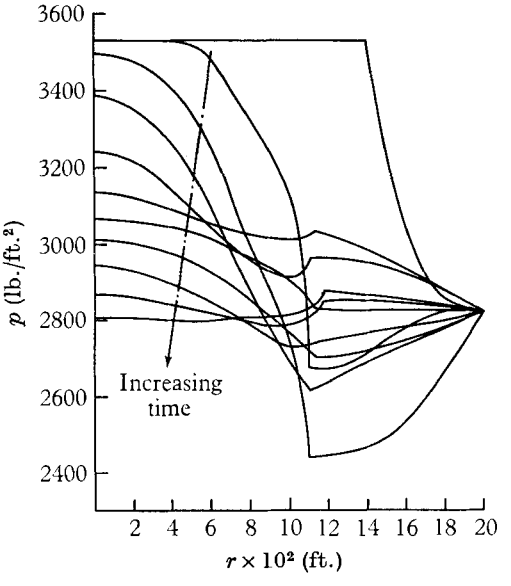

FIGURE 11. History of fluid pressure distribution.

Also of interest is the formation of a region of reduced porosity, as shown in figure 8, at a short distance behind the fibre boundary, preceded and followed by sharp changes in that quantity. This behaviour is also mirrored in figure 9 by the distributions of v_s and in figure 10 by the distributions of $v_f - v_s$. Although it is certainly not clear, one could attribute the early appearance of the plateaus in the v_s and $v_f - v_s$ distributions to the reduction in the velocity gradients in the successive air expansion wavelets which make up the initial expansion fan travelling inward from the end wall as they meet with the reflexions of the previous wavelets from the fibre sample face. Thus, the successive waves transmitted into the sample are weaker and have less and less effect. An additional consideration stems from the fact that, once the fibres move, the interaction forces, which are dependent upon $v_f - v_s$, will be reduced, so that, although the waves should penetrate the sample more easily, they should have a smaller interaction. The situation is further aggravated by the arrival at the sample face of compression waves from the end wall (cf. figure 11). These waves penetrate into the sample, reducing the relative velocity, $v_f - v_s$, (cf. figure 10) in the outermost portions below the existing level deeper within the sample. With the interaction forces thus reduced the fibre velocity does not grow as fast in this region as it does in the interior; consequently, a region of almost constant v_s continues to form somewhat behind the face of the sample. The fibre velocity at the face is much greater than that at the interior points under discussion, so that, although some reduction in the difference between velocities at these locations occurs, there still remains a considerable fibre velocity gradient just below the fibre boundary. The porosity on either side of the v_s plateau continues to increase while very little change in f occurs in this region, and, consequently, a depression in the porosity curves appears. Since the pressure waves lose their potency as they penetrate farther within the sample, and decrease in their initial strength at the end wall as the chamber pressure approaches that of the reservoir, it is expected that the region of porosity depression will remain small.

Other computations, for both smaller and similar size chambers and fibre samples, have been performed (Taub 1965); however, the permeability relation utilized was that of (9*b*) multiplied by the solidity (i.e. $(1-f)\times$ equation (9*b*)), so that for the present porosity level the permeability was about one-tenth the proper level. These calculations revealed that, instead of a depression, a porosity plateau formed at an equivalent distance below the sample face. Since air waves do not penetrate a less permeable medium as well as they do a more permeable one, this behaviour is as expected.

This paper derives from a report of the work done under contract with the U.S. Department of Agriculture and authorized by the Research and Marketing Act. This work was supervised by the Southern Utilization Research and Development Division.

REFERENCES

BIOT, M. A. 1955 *J. Appl. Phys.* **26**, 182.
BIOT, M. A. 1956 *J. Appl. Phys.* **27**, 459.
DAVIS, G. 1957 Ph.D. Dissertation, Cambridge University.
DUBOIS, W. F. 1959 *Textile Res. J.* **29**, 451.
ELDER, J. W. 1959 *J. Fluid Mech.* **5**, 355.
GRÅLEN, N. & OLAFSSON, B. 1947 *Textile Res. J.* **17**, 488.
LORD, E. 1955*a* *J. Textile Inst.* **46**, 41.
LORD, E. 1955*b* *J. Textile Inst.* (*Trans.*) **46**, T 191.
PARIA, G. 1958 *Bull. Calcutta Math. Soc.* **50**, 71.
PARIA, G. 1963 *Appl. Mech. Rev.* **16**, 421.
POSTLE, J. L., INGHAM, J. & COX, D. R. 1952 *J. Textile Inst.* (*Trans.*) **43**, T 77.
STREETER, V. L. (ed.) 1961 *Handbook of Fluid Dynamics*. New York: McGraw Hill.
TAUB, P. A. 1965 *General Applied Sc. Labs.* TR 535.